FINAL REPORT

NUMERICAL COMPUTATION OF THE FULL SET OF EQUATIONS FOR MAGNETO-FLUID DYNAMICS

AFOSR GRANT FA9550-07-1-0545

Robert W. MacCormack
Department of Aeronautics and Astronautics
Stanford University

Abstract

This report presents numerical procedures for solving the equations of Magneto-Fluid-Dynamics (MFD). These equations consist of the Navier-Stokes equations coupled to the full set of Maxwell's equations. They govern flow within electromagnetic fields. The primary interest to the Air Force of this work is flow control about aerodynamic vehicles and thrust enhancement within scramjet engines via the interaction of external electromagnetic fields, produced on board, with the high speed flow about or through the vehicle. They have been solved for both external flow and internal flow. Test cases include the Hartmann flow problem[1], weakly ionized flow simulating the RAM-C flight experiment[2], highly ionized flow past a hemi-sphere-cylindrical body simulating the Zieman experiment[3] and flow through the accelerator section of and "energy by-pass" scramjet engine[4,5].

I. Background

The interaction of an ionized flow, which caused by the flow crossing the bow shock of a high speed aerodynamic vehicle, with electromagnetic fields produced on board offers a potential breakthrough in both hypersonic vehicle design and propulsion. Reductions in heat transfer and flow control using magnetic fields can be important for enabling a hypersonic vehicle to pass more efficiently and safely through the atmosphere. Magnetic and electric fields placed within the propulsion system may enable the extraction of electrical energy from the ionized flow entering the engine, while simultaneously slowing the fluid, without losses in total pressure caused by shockwaves, and enhancing complete fuel combustion. The extracted energy can be returned back into the flow after combustion for further flow acceleration and engine thrust. Realistic aerodynamic simulations, under the conditions of expected low electrical conductivities and reasonably strong magnetic fields, will be required to determine if these potential benefits may or may not be realizable. Solutions of the complete equations governing magneto-fluid dynamics, including magnetic induction and diffusion within strong magnetic fields, are needed to perform the required flow simulations. The goal of this research has been to develop algorithms for the simulation of weakly ionized aerodynamic flows, both internal and external, within strong externally applied electromagnetic fields

The algorithms developed within this research contain numerical procedures for solving the governing MFD equations, applying boundary conditions, evaluating temperature and pressures for an open ended set of chemical species composing the flow, and determining the electrical conductivity of the ionized gas. The governing equations of MFD consist of the Navier-Stokes equations, Maxwell's equations and the equations describing chemical and thermal equilibrium

REPORT DOCUMENTATION PAGE

Form Approved
OMB No. 0704-0188

1. REPORT DATE (DD-MM-YYYY)	2. REPORT DATE	3. DATES COVERED: *(From – To)*
11-02-2010	FINAL	2007-20909

4. TITLE AND SUBTITLE

NUMERICAL COMPUTATION OF THE FULL SET OF EQUATIONS FOR MAGNETO-FLUID DYNAMICS

5a. CONTRACT NUMBER
FA9550-07-1-0545

5b. GRANT NUMBER
FA9550-07-1-0545

5c. PROGRAM ELEMENT NUMBER

6. AUTHOR(S)

Robert W. MacCormack

5d. PROJECT NUMBER

5e. TASK NUMBER

5f. WORK UNIT NUMBER

7. PERFORMING ORGANIZATION NAME(S) AND ADDRESS(ES)
Stanford University
651 Serra Street
Stanford, CA 94305

8. PERFORMING ORGANIZATION REPORT NUMBER

9. SPONSORING/MONITORING AGENCY NAME(S) AND ADDRESS(ES)
AFOSR
875 N RANDOLPH ST
ARLINGTON, VA 22203

10. SPONSOR/MONITOR'S ACRONYM(S)

AGENCY REPORT NUMBER

12. DISTRIBUTION AVAILABILITY STATEMENT
DISTRIBUTION A: Approved for Public Release

13. SUPPLEMENTARY NOTES

14. ABSTRACT
This report presents numerical procedures for solving the equations of Magneto-Fluid-Dynamics (MFD). These equations consist of the Navier-Stokes equations coupled to the full set of Maxwell's equations. They govern flow within electromagnetic fields. The primary interest to the Air Force of this work is flow control about aerodynamic vehicles and thrust enhancement within scramjet engines via the interaction of external electromagnetic fields, produced on board, with the high speed flow about or through the vehicle. They have been solved for both external flow and internal flow. Test cases include the Hartmann flow problem, weakly ionized flow simulating the RAM-C flight experiment, highly ionized flow past a hemi-sphere-cylindrical body simulating the Zieman experiment and flow through the accelerator section of and "energy by-pass" scramjet engine.

15. SUBJECT TERMS
Magneto-Fluid Dynamics, Maxwell's Equations, Hypersonic Flow, Scramjets, Non-Equilibrium Flow

16. SECURITY CLASSIFICATION OF:			17. LIMITATION OF ABSTRACT	18. NUMBER OF PAGES	19a. NAME OF RESPONSIBLE PERSON
a. REPORT	b. ABSTRACT	C. THIS PAGE			Robert W. MacCormack
U	U	U	UU	18	**20b. TELEPHONE NUMBER (include area code)** (650) 723-4627

and non-equilibrium high temperature air. Maxwell's equations appear in two forms – 1) the usual form found in the literature and 2) the scalar and vector potential form found in text books, but not attempted for solution. The present effort developed solution and boundary condition procedures for both forms and have been presented at seven AIAA (American Institute of Aeronautics and Astronautics) meetings during the last three years[6-12]. This volume of research cotributions is too large to replicate herein. Instead, the procedures will be briefly described and illustrative applications will be shown from the AIAA papers. We first present the MFD equations.

The Equations of Magneto-Fluid Dynamics

1) The Navier-Stokes equations $\frac{\partial U}{\partial t}+\frac{\partial F}{\partial x}+\frac{\partial G}{\partial y}+\frac{\partial H}{\partial z}=S$, with $U=\left[\rho,\rho u,\rho v,\rho w,e\right]^T$,

density ρ, velocities u, v and w, total energy per unit volume e.

2) Maxwell's equations - The Ampere-Maxwell equation $\frac{\partial \vec{E}}{\partial t}=\frac{1}{\varepsilon_e}\left(\frac{\vec{\nabla}\times\vec{B}}{\mu_e}-\vec{J}\right)$

Faraday's equation $\frac{\partial \vec{B}}{\partial t}=-\vec{\nabla}\times\vec{E}$

with constraints $\vec{\nabla}\cdot\vec{E}=\frac{1}{\varepsilon_e}\rho^c$ and $\vec{\nabla}\cdot\vec{B}=0$,

electric field $\vec{E}$, magnetic field $\vec{B}$, current density $\vec{J}$, inductive capacity ε_e,

magnetic permeability $\mu_e=4\pi\times10^{-7}\frac{kg\cdot m}{(coulomb)^2}$ and charge density ρ^c.

3) Generalized Ohm's law $\vec{J}=\sigma_e(\vec{E}+\vec{u}\times\vec{B})$, with electrical conductivity σ_e.

4) MFD assumption: charge neutral plasma, $\rho^c=0$.

The source term S in the Navier-Stokes equations consists of the Lorentz force, $\vec{L}_f=\vec{J}\times\vec{B}$, acting on the momentum of the flow and Joule heating, caused by the flow of electric current through the fluid, plus the magnetic force work term acting on the energy of the flow.

$$S=\left[0,(\vec{J}\times\vec{B})_x,(\vec{J}\times\vec{B})_y,(\vec{J}\times\vec{B})_z,\frac{1}{\sigma_e}\vec{J}\cdot\vec{J}+(\vec{J}\times\vec{B})\cdot\vec{u}\right]^T$$

The Magnetic Reynolds number is defined by $R_m=u_0 l_0\sigma_e\mu_e$, where u_0 and l_0 are reference flow speed. Most MFD simulations use the "Low Magnetic Reynolds" number approximation, which assumes that the electromagnetic field within the fluid changes insignificantly from that imposed externally. The approach taken here is allow the fields to change via induction as prescribed by the full set of Maxwell's equations. It will be shown that small changes to the electromagnetic field can produce significant changes to the flow. The set of Maxwell's equations above are the "usual" set found in the literature. This set consists of six field equations, plus the constraint that the magnetic field remain divergence free, $\vec{\nabla}\cdot\vec{B}=0$. The "scalar and vector potential" form of Maxwell's equations, consisting of just four field equations, and automatically satisfying the divergence free constraint, is given below.

The Scalar and Vector Potential Form of Maxwell's Equations

The excellent AIAA paper by Giordano[13] describes the governing equations of fluid dynamics within electromagnetic fields. His paper presents and derives the scalar and vector potential form of Maxwell's equations, summarized below following his description. Because the divergence of a curl is zero, it is desirable to represent $\vec{B}$ as the curl of a vector $\vec{A}$, thus automatically satisfying the constraint $\vec{\nabla}\cdot\vec{B}=0$. Substituting $\vec{B}=\vec{\nabla}\times\vec{A}$ into Faraday's equation yields

$$\frac{\partial\vec{\nabla}\times\vec{A}}{\partial t}=-\vec{\nabla}\times\vec{E} \qquad \text{or} \qquad \vec{\nabla}\times\left(\vec{E}+\frac{\partial\vec{A}}{\partial t}\right)=0$$

The term within the parenthesis is "curl free", which implies that a potential φ exists such that $\vec{E}+\frac{\partial\vec{A}}{\partial t}=-\vec{\nabla}\varphi$. Substituting this relation into Ampere's equation, $\frac{\partial\vec{E}}{\partial t}=c_e^2\vec{\nabla}\times\vec{B}-\frac{1}{\varepsilon_e}\vec{j}$, and using the identity, $\vec{\nabla}\times\vec{B}=\vec{\nabla}\times\vec{\nabla}\times\vec{A}=\vec{\nabla}(\vec{\nabla}\cdot\vec{A})-\nabla^2\vec{A}$, yields

$$-\frac{\partial(\vec{\nabla}\varphi+\frac{\partial\vec{A}}{\partial t})}{\partial t}=c_e^2\left(\vec{\nabla}(\vec{\nabla}\cdot\vec{A})-\nabla^2\vec{A}\right)-\frac{1}{\varepsilon_e}\vec{j}$$

or

$$\frac{\partial^2\vec{A}}{\partial t^2}=c_e^2\nabla^2\vec{A}-c_e^2\left(\vec{\nabla}\left\{\vec{\nabla}\cdot\vec{A}+\frac{1}{c_e^2}\frac{\partial\varphi}{\partial t}\right\}\right)+\frac{1}{\varepsilon_e}\vec{j}$$

The term in the "curly" bracket is related to the "Lorentz gauge" and is set to zero to remove the arbitrariness in the choice of the vector potential $\vec{A}$. Thus $\vec{\nabla}\cdot\vec{A}+\frac{1}{c_e^2}\frac{\partial\varphi}{\partial t}=0$ and the time dependent equation for $\vec{A}$ becomes $\frac{\partial^2\vec{A}}{\partial t^2}=c_e^2\nabla^2\vec{A}+\frac{1}{\varepsilon_e}\vec{j}$. From the constraint on the electric field, $\vec{\nabla}\cdot\vec{E}=\frac{1}{\varepsilon_e}\rho^c$, and with the substitution $\vec{E}=-\vec{\nabla}\varphi-\frac{\partial\vec{A}}{\partial t}$ from above, $-\nabla^2\varphi-\frac{\partial\vec{\nabla}\cdot\vec{A}}{\partial t}=\frac{1}{\varepsilon_e}\rho^c$, which via the "Lorentz gauge" becomes $\frac{\partial^2\varphi}{\partial t^2}=c_e^2\nabla^2\varphi+\frac{c_e^2}{\varepsilon_e}\rho^c$.

In summary, the scalar and vector potential form of Maxwell's equations are

$$\frac{\partial^2\varphi}{\partial t^2}=c_e^2\nabla^2\varphi+\frac{c_e^2}{\varepsilon_e}\rho^c \qquad \text{and} \qquad \frac{\partial^2\vec{A}}{\partial t^2}=c_e^2\nabla^2\vec{A}+\frac{1}{\varepsilon_e}\vec{j}$$

with the magnetic field $\vec{B}$ and electric field $\vec{E}$ determined from the solutions for scalar φ and vector $\vec{A}$ by

$$\vec{B}=\vec{\nabla}\times\vec{A} \qquad \text{and} \qquad \vec{E}=-\vec{\nabla}\varphi-\frac{\partial\vec{A}}{\partial t}$$

Note that only four elements need to be solved for in time, one scalar and the three components of $\vec{A}$ and also the constraint $\vec{\nabla} \cdot \vec{B} = 0$ is automatically satisfied.

Solution Procedures for the Equations of Magneto-Fluid Dynamics

Decomposing the Electromagnetic Fields into their Imposed and Induced Components

It is advantageous to decompose the electromagnetic fields into their imposed and induced parts. First, the induced fields may be orders of magnitude smaller than the imposed fields and their magnitudes may therefore be compromised in numerical precision if they remain combined during numerical operations. Second, the implementation of initial and boundary conditions becomes simpler, because the imposed conditions are fixed by conditions external to, and therefore independent of, the calculated induced flow field. Therefore, we write for the magnetic, electric, scalar and electric potentials

$$\vec{B}_t = \vec{B} + \vec{B}_0 \quad \text{and} \quad \vec{E}_t = \vec{E} + \vec{E}_0$$
$$\varphi_t = \varphi + \varphi_0 \quad \text{and} \quad \vec{A}_t = \vec{A} + \vec{A}_0$$

where the subscript t indicates the total field and the subscript 0 indicates the imposed field. The un-subscripted variables are the induced field components. Note that both forms, the usual and the scalar and vector potential forms, of Maxwell's equations are linear. Therefore, the imposed fields, $\vec{B}_0$, $\vec{E}_0$, φ_0 and $\vec{A}_0$, and the induced fields, $\vec{B}$, $\vec{E}$, φ and $\vec{A}$, each independently satisfy Maxwell's equations.

Boundary Conditions for the Electromagnetic Fields

Usually, textbooks give electromagnetic boundary conditions on what variables or derivatives are ***continuous*** across boundaries, so as relate these fields inside the flow field to those outside. However, it is desired here to calculate the electromagnetic fields only within the flow field. We therefore need the ***values*** of the electromagnetic field variables or their derivatives, the so called Dirichlet and Neumann type boundary conditions, instead of their continuity properties across boundaries. Otherwise, both the region within the flow field and outside would need to be calculated. To avoid this complication, we assume that there is sufficient information concerning the imposed fields along all boundaries of the flow field to set the needed boundary conditions. The following assumption is made along solid wall boundaries for the applications to follow.

Assumption: We assume that the boundaries at solid walls are "perfectly conducting". This implies that gradients in the electric field components parallel to the walls vanish. Otherwise, infinite currents would arise. We also assume that these components of the imposed electric field are constant in time and seek solutions converging to steady state in time.

Numerical Method for the Navier-Stokes Equations

The Navier-Stokes equations contain both the inviscid Euler and viscous terms. All terms and the boundary conditions are treated implicitly. The Euler terms use a modified Steger-Warming flux splitting procedure. The approach used herein, believed originally suggested by C. Lombard[14] in the 1980s, has the benefit of partitioning the conservative flux vectors themselves, which, for example, unlike the state vectors, are continuous across stationary discontinuities in the flow. But

more importantly, this approach can be used to partition general flux vectors that are not homogeneous of degree 1 with respect to the state vector U and does not need an approximate Riemann solution. For example, the flux at a surface between mesh points i, j and $i+1, j$ is given by

$$F^n_{i+1/2,j} = \mathcal{A}^n_{+_{i+1/2,j}} F^n_{i,j} + \mathcal{A}^n_{-_{i+1/2,j}} F^n_{i+1,j}$$

where $\mathcal{A}^n_{\pm_{i+1/2,j}}$ are matrices and $F^n_{i,j}$ and $F^n_{i+1,j}$ are fluxes at and about the flux surface $i+1/2, j$.
High order accurate approximations for the fluxes can be made by upwind extrapolation or interpolation of the flow variables to the flux surfaces. Second and third order accurate approximations are used herein along with a TVD (Total Variation Diminishing) procedure.

Numerical Method for the Maxwell Equations

(1) The Usual Form of Maxwell's Equations - The initial attempt to solve the full set of Maxwell's equations, using a similar approach to that for the Navier-Stokes equations, showed too much numerical dissipation. The source of the dissipation was found and a novel scaling of the Maxwell flux vector was able to remove this difficulty. AIAA Paper 2008-4010 describes the solution procedure for solving the usual form of Maxwell's equations.

(2) The Scalar and Vector Potential Form of Maxwell's Equations - Solution of this form of the equations was attempted because of the "four component" form of the unknowns and the automatic satisfying of the constraint that the magnetic field be divergence free. The four component form is fundamental to physical laws, i.e., Momentum and energy, where mass is a form of energy. Four component forms transform naturally in space-time, i.e., under Lorentz transformations. This form showed no solution difficulties, however boundary conditions were more complicated This work is described in AIAA Paper 2009-0455

Numerical Method for the Equations of Equilibrium and Non-Equilibrium

An air chemistry model containing nine species, plus two species for cesium and its ion, was considered. The cesium species were used to seed the flow within a scramjet engine to enhance ionization and hence the electrical conductivity of the gas. The species considered were

$$N_2, O_2, NO, N, O, e^-, N_2^+, O_2^+, NO^+, N^+, O^+, Cs \text{ and } Cs^+$$

An 11 equation reaction model for the 11 air species, plus cesium and its ion, is shown below.

(1) $N_2 + M \leftrightarrow 2N + M$
(2) $O_2 + M \leftrightarrow 2O + M$
(3) $NO + M \leftrightarrow N + O + M$
(4) $N_2 + O \leftrightarrow NO + N$
(5) $NO + O \leftrightarrow N + O_2$
(6) $N + O \leftrightarrow NO^+ + e^-$
(7) $Cs + e^- \leftrightarrow Cs^+ + e^- + e^-$
(8) $N + e^- \leftrightarrow N^+ + e^- + e^-$
(9) $O + e^- \leftrightarrow O^+ + e^- + e^-$
(10) $N + N \leftrightarrow N_2^+ + e^-$
(11) $O + O \leftrightarrow O_2^+ + e^-$

A three temperature model for translational ,rotational and vibrational temperatures was used to determine the thermal non-equilibrium of the gas. This work is described in AIAA Paper 2010-0225.

Applications

All results shown below were obtained with the numerical procedures discussed above. The procedures and the boundary conditions were fully implicit and run to high CFL numbers (10^5) limited only by numerical precision considerations. Each problem was run to steady state in less than 256 time steps on a lap top computer.

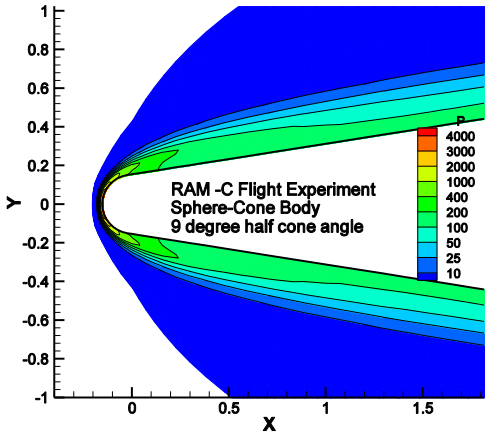

Ram-C Flight Experiment Figure 1 RAM-C flow field pressure contours

During the 1960's a series of flight experiments[2] were made at high altitudes during which electron number densities were measured using microwave reflectometers. The vehicle was a sphere-cone body, with a 9^o cone half angle and a length of 1.295m. The simulated flow field about the body nose is shown in Figure 1 above, showing pressure contours for a free stream (shown in solid blue) of Mach 25.9 at an altitude of 71km.

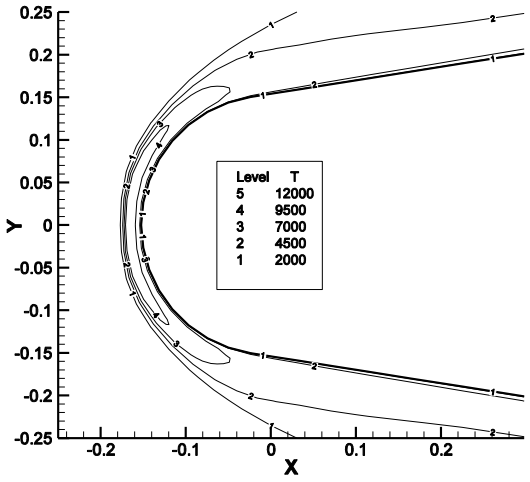

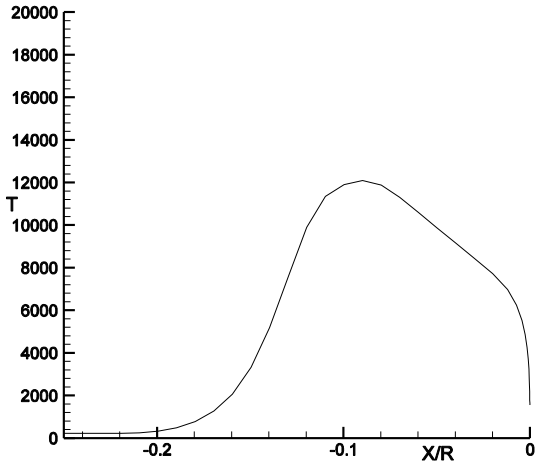

Figure 2 Temperature contours, RAM-C **Figure 3** T along stagnation streamline

The present case was chosen as a test case to check the results using non-equilibrium chemistry model 1 using 7 species, $N_2, O_2, NO, NO^+, N, O \text{ and } e^-$. Cesium was included but played no part because the initial mass concentrations were set to zero. A single energy equation was solved for temperature. Temperature contours and the temperature along the stagnation streamline are shown in Figures 2 and 3. Species mass fractions, $c_s = \rho_s / \rho$, are shown in Figure 4. Peak electron densities, within the shock layer around the body, are compared in Figure 5. The comparison between experiment, shown by the symbols, and computation is fairly good. This simulation was made twenty years earlier by Candler[15] with excellent agreement. Electron contours are shown in Figure 6. Mass fractions contours for atomic nitrogen and oxygen are shown in Figs. 7 and 8.

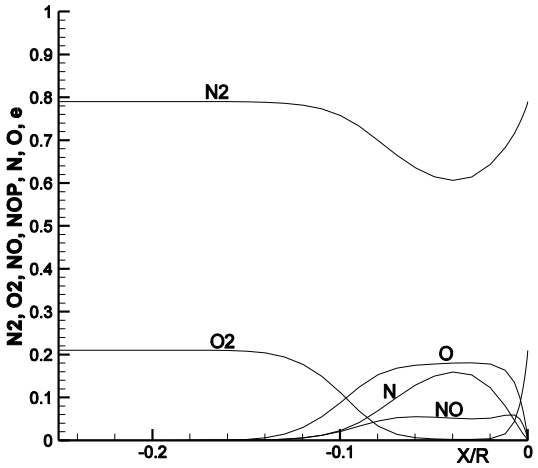

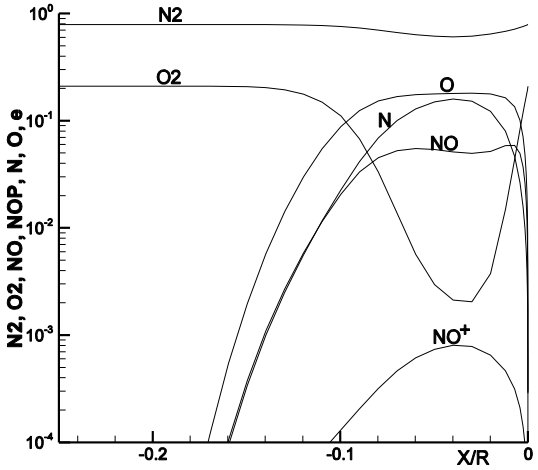

Figure 4(a) Mass fractions along stagnation streamline, **(b)** Mass fractions on log plot

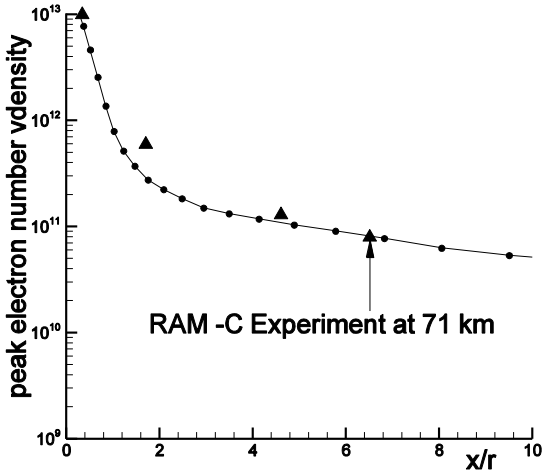

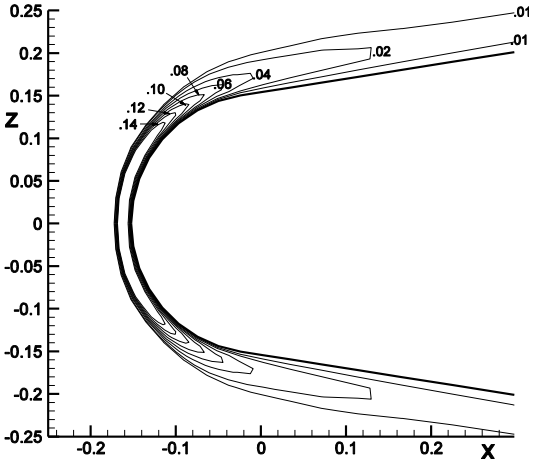

Figure 5 Peak electron number density **Figure 6** Electron mass fractions $c_e \times 10^7$

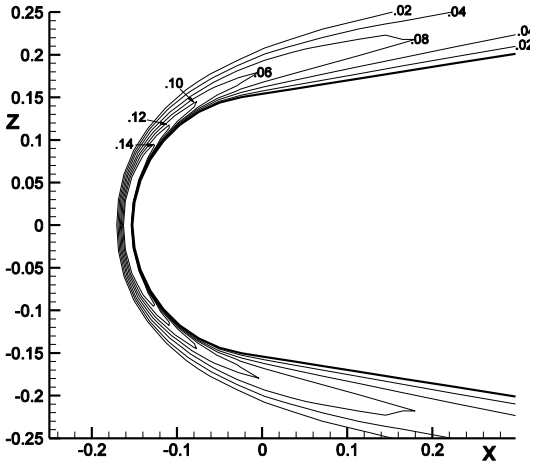

Figure 7 Contours of N mass fractions

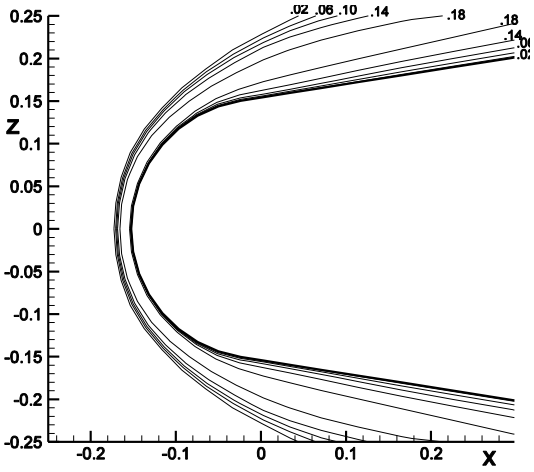

Figure 8 Contours of O mass fractions

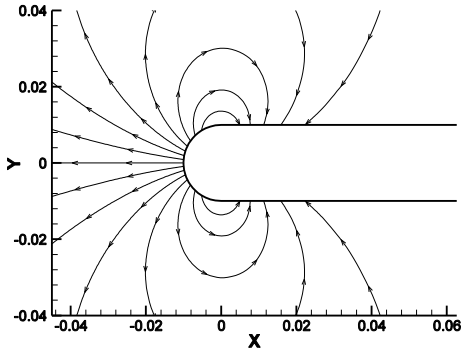

Figure 9 Dipole magnetic field lines

Results for the Ziemer Experiment

In 1959 R.W. Ziemer[2] reported results from an experimental investigation in magneto-aerodynamics. He placed a hemi-spherically nosed cylinder, of diameter 0.02m and made of Pyrex glass, within an electromagnetic shock tube. A blast wave moved at Mach 21.5 into stationary air, at temperature 273^{o} K and pressure 9.33N/m^2, past the model, producing a hypervelocity flow of ionized air. The period of steady flow time was only about 10 to 20 microseconds. He placed a coaxial pulsed magnetic copper coil within the nose of the body, which produced a dipole magnetic field of 4 Tesla at the stagnation point of the body. He observed that with the magnetic field turned on the shock wave standoff distance increased by a factor of 7.5 for a magnetic interaction parameter $Q = \sigma_e B_0^2 l_0 / \rho_\infty u_\infty$ =69. The free stream conditions for the present Ziemer flow simulation are given in the table below. Although an attempt was made to match the experimental conditions of Ziemer, no precise match for the magnetic interaction parameter Q could be made because of the large variation in electrical conductivity σ_e behind the shock. There was no clear choice of which value to use. The imposed magnetic field at the stagnation point was either B_o=0 or 5 Tesla. The temperature behind the shock wave near the nose was about 20,000^{o}K and pressures were as high as 9x10^4 N/m^2. At these conditions the flow was almost completely dissociated. The non-equilibrium chemistry model included both the seven and eleven species model for non-equilibrium air. A single temperature was used in the present simulation, again using Park's[4] thermodynamic relations. An

isothermal wall boundary condition was assumed with the wall temperature at 273^{o}K. However, a catalytic boundary condition[16] for both species and internal energy was used at the wall.

Free Stream Conditions

velocity	6715 m/s
pressure	5717 N/m^2
temperature	6049 ^{o}K
density	2.011x10^{-3}kg/m^3

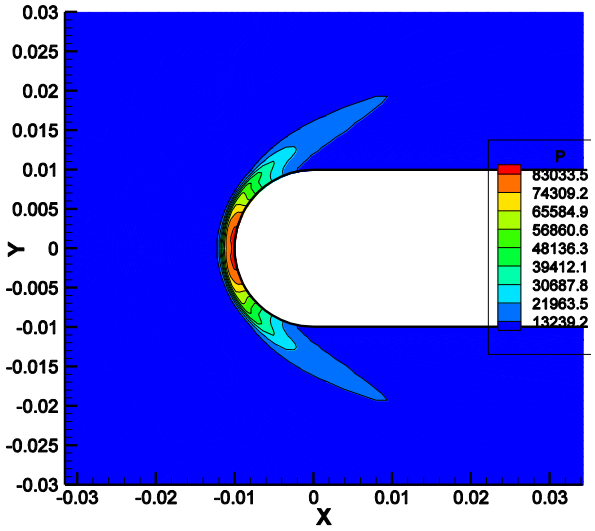

Figure 10 Pressure contours, B_o=0, 7 species air

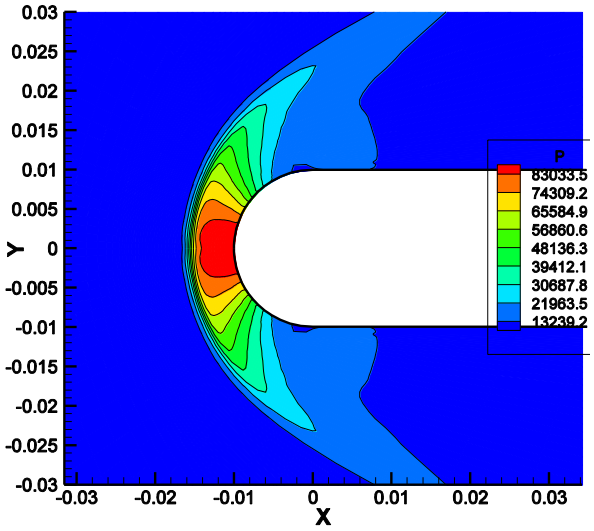

Figure 11(a) Pressure contours, B_o=5, 7 species air

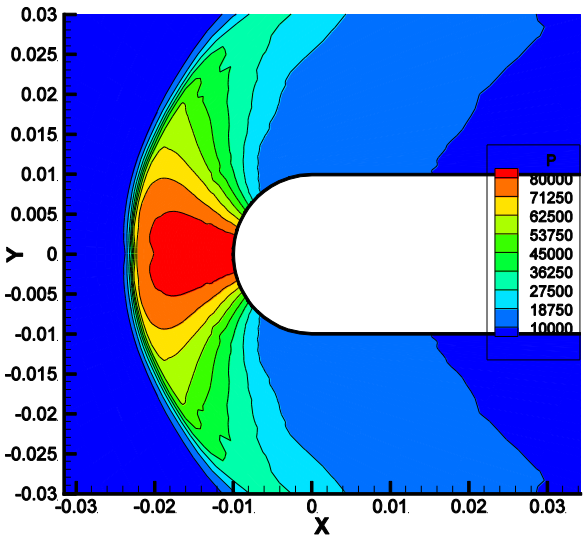

Figure 11(b) Pressure contours, B_o=5, 11 species air

Standoff Distance

The pressure contours for the flow about the model are shown above in Figs.10, 11(a) and (b), with and without the dipole magnetic field and using the 7 and 11 species model for non-

equilibrium air. When the magnetic field was turned on, the standoff distance of the bow shock wave from the model nose increased from 0.0017m to 0.0058m, a factor 3.4 times further, for the 7 species air model, and to 0.0231m for the 11 species model, a factor 7.7 times greater than that shown in Fig.10. The 11 species model of air included ionization of N_2, O_2, N *and* O as well as NO, which increased the number of free electrons and therefore the electrical conductivity of the gas and the electromagnetic field interaction with the flow. The 11 species air model is more realistic for simulating Zieman's experiment because the temperatures behind the bow shock wave reach temperatures as high as 20,000^o K.

Imposed and Induced Magnetic Fields

The imposed and induced x components of the magnetic fields surrounding the sphere-cylinder body are shown below. It is observed that the induced field strengths are small compared to those imposed and therefore the *Low Magnetic Reynolds* number approximation would probably suffice. Also, it is interesting to note that in Figures 12 and 13(a) and (b) the induced field tends to reduce the total field strength.

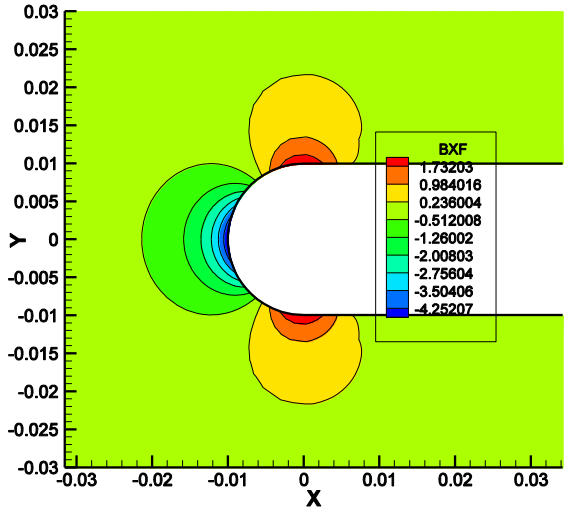

Figure 12 Imposed B_{0_x} field

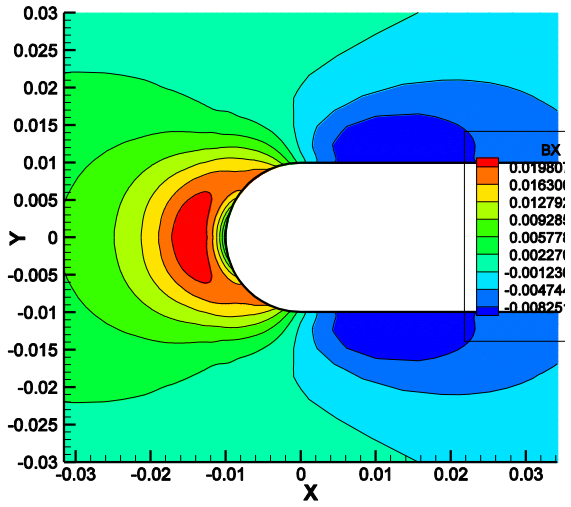

Figure 13(a) Induced B_x field, 7 species air

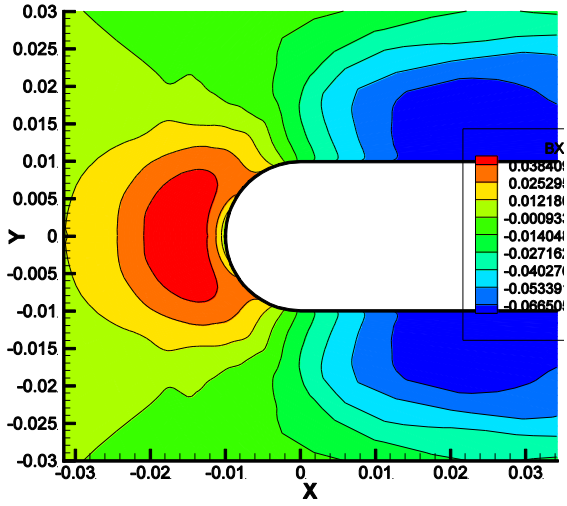

Figure 13(b) Induced B_x field, 11 species air

Mass Fractions and Temperature along Stagnation Streamline

Mass fractions along the stagnation streamline are shown in Figure 14 below for the case with the magnetic field turned on for the seven species air model. The plot at the left is linear and that on the right is a log plot. At the high free stream temperature diatomic oxygen is near completely dissociated.

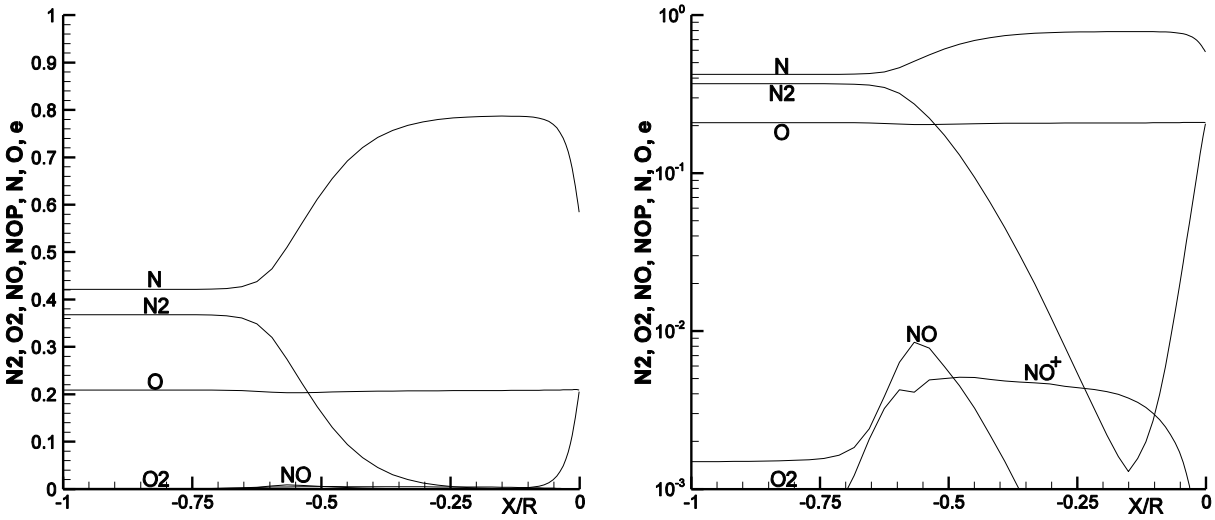

Figure 14 Mass Fractions ρ_s / ρ along stagnation stream line, left - linear and right - log plots

The temperature along the stagnation streamline is shown below in Figure 15, again for the 7 species model for air.

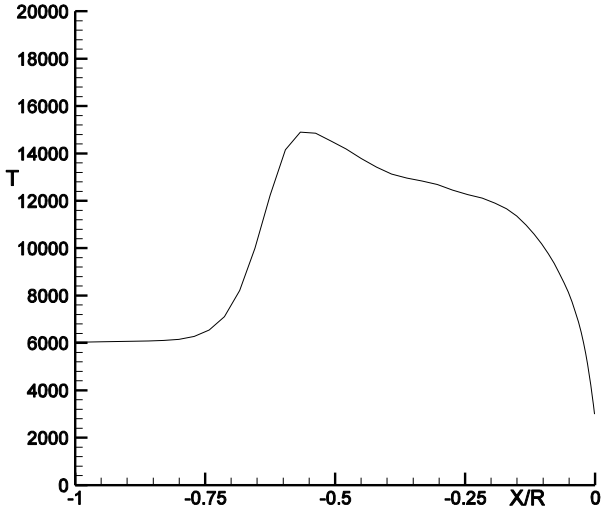

Figure 15 Temperature along stagnation streamline

Computational Results for the Hartmann Problem

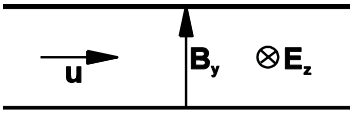

Figure 16 Hartmann Flow

An appropriate first test case for the MFD equations is Hartmann Flow[1]. Hartmann flow consists of viscous flow between two infinite parallel plates within an imposed constant magnetic field, $B_{y_0} > 0$, normal to the plates and an imposed electric field, $E_{z_0} < 0$, normal to the flow and the imposed magnetic field. A stream wise pressure gradient, $\frac{\partial p}{\partial x}$, is also imposed upon the flow. All other derivatives with respect to x, as well as all those for z, vanish. Analytic solutions exist for velocity u and induced magnetic field component B_x as functions of y. The Hartmann number is defined by $R_H = \sqrt{\frac{\sigma_e}{\mu_0}} B_{y_0} y_h$, where μ_0 is the fluid viscosity and y_h is half the distance between the plates. The electrical load factor is defined by $L = -\frac{E_{z_0}}{u_0 B_{y_0}}$. The mass flow rate $\int_{-y_h}^{y_h} u \, dy = 2u_0 y_h$ is held constant during the calculation, i.e. the average velocity across the channel is u_0. Initially the current has only a z component, $J_z = \sigma_e \left(E_{z_0} + u B_{y_0} \right)$. The Lorentz force acting on the fluid, $\vec{L}_f = \vec{J} \times \vec{B}$, has x component $L_{fx} = -J_z B_{y_0} = -\sigma_e B_{y_0} \left(E_{z_0} + u B_{y_0} \right)$. Hence, the average force across the channel is $L_{fx} = -u_0 \sigma_e B_{y_0}^2 \left(\frac{E_{z_0}}{u_0 B_{y_0}} + 1 \right)$. Thus, load factors greater than one will accelerate the flow and those less than one will decelerate the flow. This force, as well as the viscous friction forces, must be balanced by the pressure gradient, $\frac{\partial p}{\partial x} = -u_0 \sigma_e B_{y_0}^2 \left(\frac{E_{z_0}}{u_0 B_{y_0}} + \frac{R_H}{R_H - \tanh(R_H)} \right)$, where the Hartmann number dependence is caused by viscous forces.

Computed results for the full set of MFD equations are compared with the analytical solution in Figure 17. The initial flow was at Mach 0.1, at atmospheric pressure and 300^o K temperature. A perfect gas equation of state was assumed. The plates were isothermal, also at 300^o K, and the Hartmann number was 10. The electrical conductivity σ_e was determined from the Hartmann number relation given above. The distribution of B_x is anti-symmetric across the channel and the velocity u is symmetric. The numerical solution of the usual form of Maxwell's equations, (filled circle symbols) and those of the potential form, (open square symbols) are both in excellent agreement with theory[1] (line). The results shown locked in after 128 time steps, but the calculation was continued to 2048 time steps without further change.

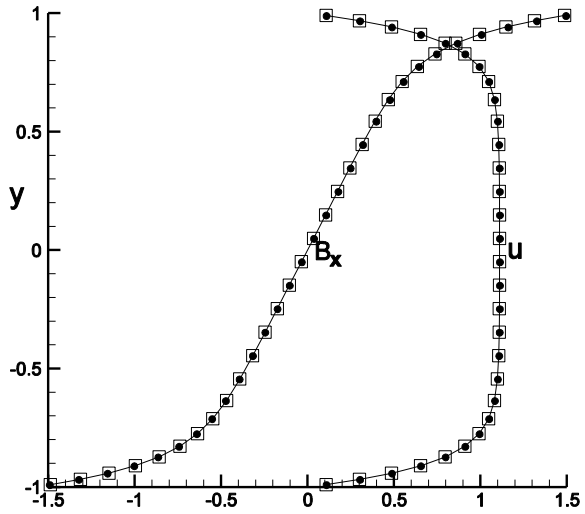

Figure 17 Hartmann Flow Solutions Compared with Theory, symbols-numerical, curve-theory

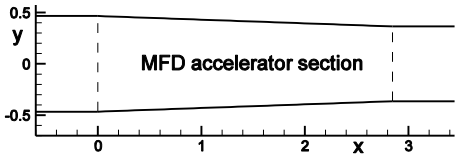

Computational Results for an MFD Accelerator

Figure 18 Sketch of MFD channel accelerator

Park, Bogdanoff and Mehta[4] presented a 1-D analysis of the performance of a scramjet propulsion system incorporating the MFD (magneto-fluid dynamics) energy bypass concept[3]. The system contained sections for an MFD generator, combustor and an MFD accelerator. The Park, Bogdanoff and Mehta accelerator section was a square converging duct, 2.846m long, of height/width 0.933m at the entrance and 0.730m at the exit, which is sketched in Figure 18. It is located just down stream of the combustor section. The imposed magnetic field across the channel was $B_{0_y} = 11.28$T and the transverse voltage gradient varied from E_{0_z} = -30,990 V/m at the entrance to -31,470 V/m at the exit. At the entrance the pressure was 1.251x10^6 N/m^2, temperature 3583^o K, and the Mach number equaled 1.15. The electrical conductivity used by Park, Bogdanoff and Mehta was $\sigma_e = 35.87 mho/m$. The interaction parameter $Q = \sigma_e B_0^2 l_0 / \rho_\infty u_\infty$ =20 and the magnetic Reynolds number R_m =0.17, defined by $R_m = u_0 l_0 \sigma_e \mu_e$, where u_0 and l_0 are reference flow speed and accelerator channel length, and μ_e is the magnetic permeability.

In the present study, the flow is treated as two dimensional and σ_e is calculated. Laplace's equation for the imposed electro-magnetic fields within the channel was solved to keep $\vec{\nabla} \times \vec{B}_0 = 0$. The non-equilibrium chemistry model contained 9 species, $N_2, O_2, NO, NO^+, N, O, Cs, Cs^+ and\ e^-$, including cesium and its ion with initial mass fractions of 4x10^{-4} and 0, respectively. Maxwell's equations were solved[3] in their vector potential form. The electrical conductivity depended upon the degree of ionization present and was calculated

via Park's transport model[17]. The rate constants for cesium came from Park[18] citing the experimental data of Chen, C.J., Wu, J.M., Wu, F.T., and Shaw, D.T[19].

The components of the induced and imposed magnetic and electric fields, some showing field lines, are shown in Figures 19 to 24. The induced fields are very small compared with the imposed fields, particularly the electric field. A supersonic flow in a converging channel should slow down, but the results shown in Figures 25 show considerable acceleration of the flow, caused by the interaction of the electromagnetic fields with the ionized flow. These results are similar to those obtained for flows simulated with equilibrium gas chemistry[15]. The maximum temperature within the flow was about 4,400^{o} K and the flow reached chemical equilibrium. The solution converged in about 200 time steps.

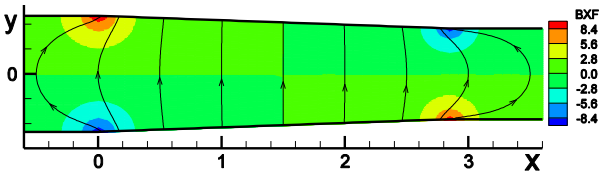

Figure 19 Imposed B_{0_x} field

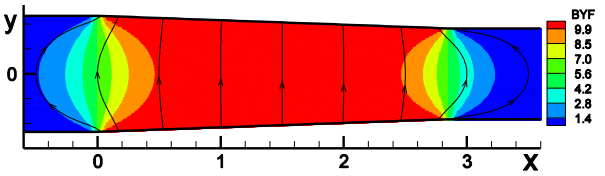

Figure 20 Imposed B_{0_y} field

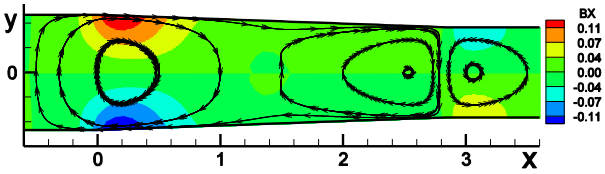

Figure 21 Induced B_x field

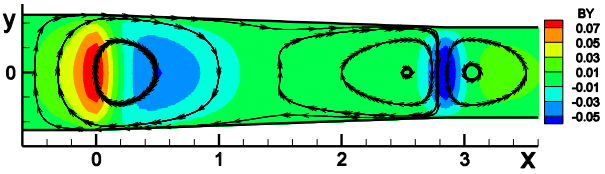

Figure 22 Induced B_y field

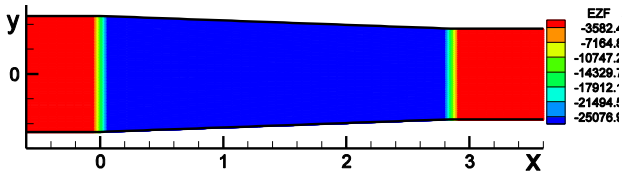

Figure 23 Imposed E_{0_z} field

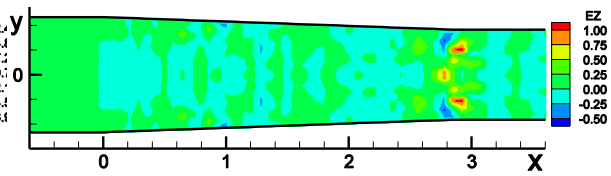

Figure 24 Induced E_z field

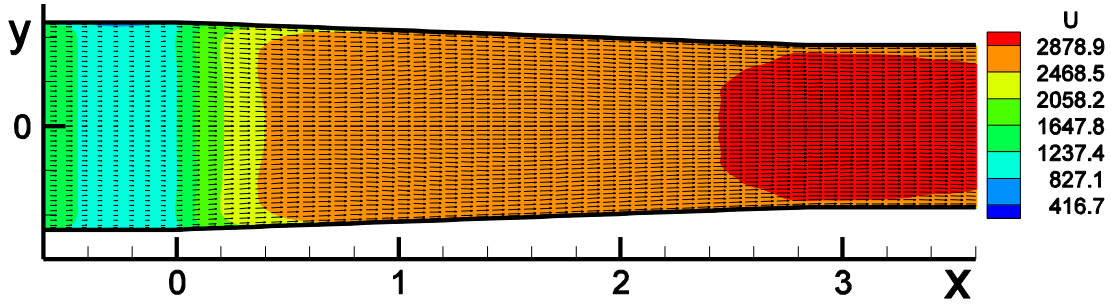

Figure 25 Velocity vectors and u velocity contours

Thrust, Velocity and the Unstart Problem

Figure 26 shows accelerator section thrust and maximum velocity along the channel.

$$Thrust = \frac{\int_{S(exit)} \left(\rho u^2 + p\right) ds}{\int_{S(entrance)} \left(\rho u^2 + p\right) ds} \quad \text{and} \quad u_{\max} = \frac{1}{u_0} \max_{y,z} \{u(x, y, z)\}$$

The velocity increases by a factor of more than two, in agreement with the load factor setting, and the thrust by more than 50%. However, a shock wave is seen moving back up the channel, located at about x = -0.5 in the figure, which will cause the engine to unstart. The design Mach number at the entrance of 1.15 cut it too close and a larger Mach number is needed as a safety factor to prevent an engine unstart. The accelerator section of the channel is 2.846m long, starting at x=0. Note the peak in velocity at the end of the section, where the imposed magnetic field decreases, as shown in Figure 20. Apparently, there is also a defect in velocity at the start of the accelerator section, where the imposed magnetic field increases, which causes the flow to be subsonic, starting a shock wave to form, which moves forward as observed in the figure above. This phenomenon was also observed in equilibrium flow simulations[9]. The explanation for this follows.

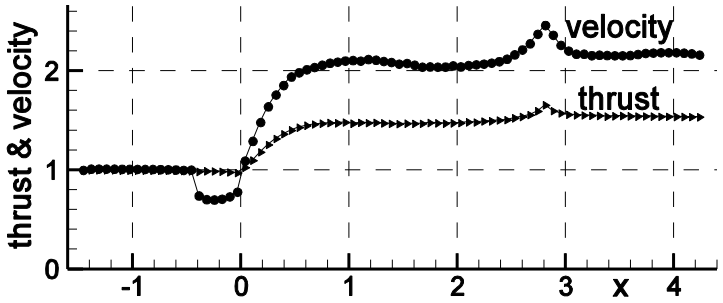

Figure 26 Accelerator Section Thrust and Velocity

The Lorentz force acting on the fluid is given by $\vec{F}_L = \vec{J} \times \vec{B}$, where $\vec{J} = \sigma_e(\vec{E} + \vec{u} \times \vec{B})$. If $\vec{E} = 0$ the Lorentz force always acts to decelerate the flow. The imposed electric field is chosen to oppose this deceleration and, if sufficiently large, accelerate the flow. Examination of Figures 18 and 21 shows that as the flow approaches the accelerator exit at x=2.846m the imposed magnetic field decreases and the electric field remains constant, thus favoring acceleration. After passing through the exit, the electric field suddenly vanishes, thus favoring deceleration and explaining the velocity peak at the accelerator exit. On the other hand, as the flow approaches the accelerator entrance at x=0, the imposed magnetic field increases and the electric field is zero, thus favoring deceleration. After passing through the accelerator entrance, the electric field suddenly increases, thus causing acceleration of the flow.

Conclusion

The goal of the present research is to develop the numerical procedures for solving the equation of magneto-fluid dynamics. This work is important to the Air Force to determine the potential benefits of the interaction of electromagnetic fields produced on board an aerodynamic vehicle

with the high speed flow about the vehicle or through its engines. The primary application of this research is to simulate flows necessary to design hypersonic vehicles. The equations governing ionized hypersonic flow include the Navier-Stokes equations, Maxwell's equations and the equations of chemical and thermal non-equilibrium. The present paper summarizes the past three year effort for solving these equations. The details of this research are contained in seven papers presented during this time at meetings of the AIAA

The procedures were applied to the RAM-C flow test problem, the Ziemer experiment, the Hartmann flow problem and to the flow within an MFD channel accelerator containing strong imposed electric and magnetic fields. The RAM-C flow case demonstrated the accuracy of the non-equilibrium flow solver. The Ziemer flow simulation agrees with the experimental finding that the standoff distance of the bow shock wave can increase several fold because of the interaction of a magnetic field with the ionized flow. The Hartmann flow problem verified the accuracy of the procedure used to solve Maxwell's equations.

.

The MFD channel accelerator cases demonstrated

1) the capability of the non-equilibrium flow procedure to include cesium as a seeding material to increase the ionization of the air gas mixture and therefore the interaction of the flow with the imposed electromagnetic field, and
2) the need for a high enough supersonic Mach number at the entrance of the accelerator to prevent an engine unstart.

Acknowledgment/Disclaimer

This work was sponsored (in part) by the Air Force Office of Scientific Research, USAF, under grant/contract number FA9550-04-1-0155. The views and conclusions contained herein are those of the authors and should not be interpreted as necessarily representing the official policies or endorsements, either expressed or implied, of the Air Force Office of Scientific Research or the U.S. Government.

References

[1]Mitchner, M., and Kruger, C.H. Jr., *Partially Ionized Gases*, 1973, John Wiley and Sons, Inc.

[2]Granthan, W.L. (1970) 'Flight results of 25,00 foot per second reentry experiment using microwave reflectometers to measure plasma electron density and standoff distance.' *NASA TN D-6062*.

[3]Ziemer, R.W.,, "Experimental Investigation in Magneto-Aerodynamics," *ARS Journal*, Vol. 29, Sept. 1959, pp. 642, 647.

[4]Gurijanov, E.P. and Harsha, P.T., ``AJAX, New Directions in Hypersonic Technology," *AIAA Paper No.~96--460*9, 1996.

[5]Park, C., Bogdanoff, D. and Mehta, U., 'Theoretical Performance of a Nonequilibrium MHD Bypass Scramjet," AIAA Paper No. 2001-0792, January 2001.

[6]*MacCormack, R.W., "*Numerical Simulation of Aerodynamic Flow within a Strong Magnetic Field with Hall Current and Ion Slip*," AIAA Paper 2007-4370, June 2007.*

[7]MacCormack, R.W., "Flow Simulations within Induced Strong Magnetic Fields," AIAA Paper 2008-1070, January 2008.

[8]*MacCormack, R.W., "*Flow Simulations within Strong Magnetic Fields*," AIAA Paper 2008-1070, June 2008.*
[9]MacCormack, R.W., "Flow Simulations within Induced Strong Magnetic Fields," AIAA Paper 2009-0455, January 2009.
[10]MacCormack, R.W., "Solution of Maxwell's Equations Coupled to the Navier-Stokes Equations," AIAA Paper 2009-3911, June 2009.
[11]MacCormack, R.W., "Algorithm Development for Hypersonic Flow," AIAA Paper 2009-7320, October 2009.
[21]*MacCormack, R.W., "*Non-Equilibrium Ionized Flow Simulations within Strong Electro-Magnetic Fields *," AIAA Paper 2010-0455, January 0225.*
[13]Giordano, D., "Hypersonic Flow Governing Equations with Electromagnetic Fields," AIAA Paper 2002-2165, June 2002.
[14]Lombard, C.K., Bardina, J., Venkatapathy, E. and Oliger, J. 'Multidimensional formulation of CSCM – an upwind flux eigenvector split method for the compressible Navier-Stokes equations.' *AIAA Paper 83-1895, Proc. AIAA 6th Computational Fluid Dynamics Conference*, pp 649-664.
[15]Candler, G.V., The Computation of Weakly Ionized Hypersonic Flows in Thermo-Chemical Nonequilibrium, PhD Thesis, Department of Aeronautics and Astronautics, Stanford University, 1988.
[16]Gokcen, T., Computation of Hypersonic Low Density Flows with Thermochemical Nonequilibrium, PhD Thesis, Department of Aeronautics and Astronautics, Stanford University, 1989.
[17]Park, C, *Nonequilibrium Hypersonic Aerothermodynamics*, 1990, John Wiley and Sons, Inc.
[18]*Trnpt* computer program obtained by author from C. Park at NASA Ames Research Center
[19]Chen, C.J., Wu, J.M., Wu, F.T., and Shaw, D.T., Journal of Applied Physics, Vol.44, No. 7, pp3052-3054, July 1973

Personnel Supported During Duration of Grant
2 PhD and 4 Master Degree Graduate Students, Stanford University

Publications
MacCormack, R.W., "Flow Simulations within Induced Strong Magnetic Fields," AIAA Paper 2008-1070, January 2008.[7]MacCormack, R.W., "*Flow Simulations within Strong Magnetic Fields*," AIAA Paper 2008-1070, June 2008.
MacCormack, R.W., "Flow Simulations within Induced Strong Magnetic Fields," AIAA Paper 2009-0455, January 2009.
MacCormack, R.W., "Solution of Maxwell's Equations Coupled to the Navier-Stokes Equations," AIAA Paper 2009-3911, June 2009.
MacCormack, R.W., "Algorithm Development for Hypersonic Flow," AIAA Paper 2009-7320, October 2009.
*MacCormack, R.W., "*Non-Equilibrium Ionized Flow Simulations within Strong Electro-Magnetic Fields *," AIAA Paper 2010-0455, January 0225.*

Honors & Awards Received
none

AFRL Point of Contact
Dr. Datta Gaitonde, AFRL/VA, WPAFB, OH.

Transitions
Computer code and numerical procedures developed herein are now used by various university researchers sponsored by AFOSR.

New Discoveries
No patents pending